Received: 10 August 2021

DOI: 10.1002/mop.33063

WILEY

RESEARCH ARTICLE

Linear calibration-free wavelength modulation spectroscopy

Renjie Li[1,2] | **Fei Li**[1] | **Xin Lin**[1] | **Xilong Yu**[1,2]

[1]State Key Laboratory of High Temperature Gas Dynamics, Institute of Mechanics, Chinese Academy of Science, Beijing, China

[2]School of Engineering Science, University of Chinese Academy of Sciences, Beijing, China

Correspondence
Fei Li, State Key Laboratory of High Temperature Gas Dynamics, Institute of Mechanics, Chinese Academy of Science, Beijing 100190, China.
Email: lifei@imech.ac.cn

Funding information
National Natural Science Foundation of China, Grant/Award Numbers: 12072355, 11802315, 11927803; Youth Innovation Promotion Association of the Chinese Academy of Sciences, Grant/Award Number: 2018023

Abstract

This article presents a new linear calibration-free wavelength modulation spectroscopy (LCF-WMS) technique for gas sensing. By combining the natural logarithms of the transmitted intensity and background signals, this technique eliminates the effects of the intensity, intensity modulation, and the modulation phase to obtain integrable harmonic signals along the line-of-sight and thus realize calibration-free measurements. To illustrate the validity of the LCF-WMS technique, it was applied to measurement of the water vapor concentration in air at ambient temperature. Because of its specific features of line-of-sight integrability and baseline independence, this method will be advantageous in absorption tomography and high-pressure applications.

KEYWORDS

calibration-free, laser spectroscopy, linear, tunable diode laser absorption spectroscopy, wavelength modulation spectroscopy

1 | INTRODUCTION

Tunable diode laser absorption spectroscopy (TDLAS) is an efficient quantitative gas monitoring technique that has been used widely in various industrial and research fields for many years.[1–4] The technique includes two main branches: direct absorption spectroscopy (DAS) and wavelength modulation spectroscopy (WMS). The DAS approach has a clear physical concept and involves a simple operation. In combination with computed tomography (CT), DAS has been used to develop the direct absorption-tunable diode laser absorption tomography (DA-TDLAT) method that can perform two-dimensional measurements.[5,6] However, low-frequency noise and baseline-fitting errors combine to restrict the measurement accuracy of DAS. The baseline dependence restricts the application of DAS under high pressure conditions.[7] To suppress the low-frequency noise, WMS realizes second harmonic peak measurement through high-frequency modulation, which also improves the signal-to-noise ratio (SNR). However, the conventional WMS technique is only applicable to weak absorbance (typically lower than 0.05) and must calibrate the second harmonic peak with respect to standard gases at known concentrations.[8,9] This is quite difficult in most practical applications because of the unstable gases involved and the in situ background signal.

To break through these limitations of WMS, researchers have developed various calibration-free wavelength modulation spectroscopy (cf-WMS) methods.[10–17] The most popular cf-WMS approach is based on normalization of the kf signal using the $1f$ signal ($kf/1f$-WMS) to remove the former signal's dependence on the DC intensity.[12,13] The gas temperature and concentration can be determined directly by comparing the experimental harmonic signals with corresponding theoretical signals. This approach has shown good results in strong absorption and high-pressure environments.[12,13,18] However, uncertainties in the laser characteristic parameters, including the intensity modulation (IM) amplitude, the frequency modulation (FM) amplitude, and the modulation phase (MP, including the IM phase and FM phase), induce discrepancies between the simulated and measured results, thus leading to measurement uncertainties that is difficult to evaluate. The distortion of the harmonic signal by the coupling of non-uniformity and laser characteristic also causes systematic errors that are difficult to evaluate in the measurement results. Simulations combining WMS with CT have proved the superiority of WMS-TDLAT technology.[19,20] However, the $kf/1f$-WMS harmonic signals are nonlinear and line-of-sight (LOS) measurements do not represent the integrals of any physical quantity, which limits the combined application of WMS with the classical CT method.[21] In recent research, a new branch of the WMS method was proposed—natural

logarithm wavelength modulation spectroscopy (ln-WMS). Li and Sun used the natural logarithm of the transmitted intensity to study the linear relationship between the second harmonic peak/amplitude and the path-integrated concentration of the absorber, with no limitations on the absorbance.[22,23] However, this method requires calibration, relies on use of the non-absorption region to obtain the demodulated phase, and does not consider the nonlinear effect of the absorption line shape under high-concentration conditions.[24]

In this article, a new WMS technique called linear calibration-free wavelength modulation spectroscopy (LCF-WMS) is proposed. Through an extended analysis of ln-WMS that involved separation of the laser intensity characteristics, the effects of both IM and MP are eliminated. It permits uncertainty quantification and a harmonic signal that can be integrated along the LOS is acquired, and calibration-free measurement is thus realized. We will verify the feasibility and accuracy of the technique through the water vapor concentration measurement experiment in air at ambient temperature.

2 | METHODOLOGY

When the wavelength modulation model that includes higher-order harmonic terms is considered, the frequency modulation and intensity modulation can be written as[18]:

$$\boldsymbol{\nu}(\boldsymbol{t}) = \overline{\boldsymbol{\nu}}(\boldsymbol{t}) + \boldsymbol{a}(\boldsymbol{t})\boldsymbol{cos}(2\boldsymbol{\pi ft} + \boldsymbol{\psi}) \tag{1}$$

$$\boldsymbol{I}_0(\boldsymbol{t}) = \overline{\boldsymbol{I}}_0(\boldsymbol{t})\left[1 + \sum_{\boldsymbol{m}=1}^{\infty} \boldsymbol{i}_{\boldsymbol{m}}(\boldsymbol{t})\boldsymbol{cos}(\boldsymbol{m} \times 2\boldsymbol{\pi ft} + \boldsymbol{\psi}_{\boldsymbol{m}})\right] \tag{2}$$

where $\overline{\boldsymbol{\nu}}(\boldsymbol{t})(\mathrm{cm}^{-1})$ is the center wavelength (or frequency) of the laser without modulation, $\boldsymbol{a}(\boldsymbol{t})(\mathrm{cm}^{-1})$ is the FM amplitude, $\boldsymbol{\psi}$ is the FM phase, and f is the modulation frequency; these four parameters constitute the laser time-frequency response relationship. $\overline{\boldsymbol{I}}_0(\boldsymbol{t})$ is the incident laser intensity without modulation, $\boldsymbol{i}_{\boldsymbol{m}}(\boldsymbol{t})$ is the mth Fourier coefficient of the IM, and $\boldsymbol{\psi}_{\boldsymbol{m}}$ is the mth-order IM phase.

When a laser beam travels through an absorbing medium, the transmitted intensity ($\boldsymbol{I}_{\boldsymbol{t}}(\boldsymbol{t})$) is described using the Beer–Lambert law[3]:

$$\boldsymbol{I}_{\boldsymbol{t}}(\boldsymbol{t}) = \boldsymbol{G}\boldsymbol{I}_0(\boldsymbol{t}) \times \boldsymbol{exp}(-\boldsymbol{A} \times \boldsymbol{\phi}[\boldsymbol{\nu}(\boldsymbol{t}), \boldsymbol{T}, \boldsymbol{P}, \boldsymbol{X}]) \tag{3}$$

$$\boldsymbol{A} = \boldsymbol{PXS}(\boldsymbol{T})\boldsymbol{L} \tag{4}$$

where G is the electro-optical gain of the detector, A is the integrated absorbance, $\boldsymbol{\phi}$ is the line shape function, P is the total gas pressure, X is the mole fraction of the absorber, S (T) is the line strength corresponding to the temperature T, and L is the absorption optical path length.

By taking the natural logarithm of the transmitted light intensity, Equation (3) can be written as:

$$\boldsymbol{ln}(\boldsymbol{I}_{\boldsymbol{t}}(\boldsymbol{t})) = \boldsymbol{ln}\left(\boldsymbol{G}\overline{\boldsymbol{I}}_0(\boldsymbol{t})\right) + \boldsymbol{ln}\left[1 + \sum_{\boldsymbol{m}=1}^{\infty} \boldsymbol{i}_{\boldsymbol{m}}(\boldsymbol{t})\boldsymbol{cos}(\boldsymbol{m} \times 2\boldsymbol{\pi ft} + \boldsymbol{\psi}_{\boldsymbol{m}})\right] - \boldsymbol{A} \times \boldsymbol{\phi}[\overline{\boldsymbol{\nu}}(\boldsymbol{t}) + \boldsymbol{a}(\boldsymbol{t})\boldsymbol{cos}(2\boldsymbol{\pi ft} + \boldsymbol{\psi}), \boldsymbol{T}, \boldsymbol{P}, \boldsymbol{X}] \tag{5}$$

The transmitted intensity becomes the linear superposition of the electro-optical gain intensity term $\boldsymbol{I}_1 = \boldsymbol{ln}\left(\boldsymbol{G}\overline{\boldsymbol{I}}_0(\boldsymbol{t})\right)$, the IM characteristic term $\boldsymbol{I}_2 = \boldsymbol{ln}\left[1 + \sum_{\boldsymbol{m}=1}^{\infty} \boldsymbol{i}_{\boldsymbol{m}}(\boldsymbol{t})\boldsymbol{cos}(\boldsymbol{m} \times 2\boldsymbol{\pi ft} + \boldsymbol{\psi}_{\boldsymbol{m}})\right]$, and the absorption signal term $\boldsymbol{I}_3 = \boldsymbol{A} \times \boldsymbol{\phi}$ (which includes the absorption signal (detection target) and the time-frequency response relationship ($\overline{\boldsymbol{\nu}}(\boldsymbol{t})$, $\boldsymbol{a}(\boldsymbol{t})$, and $\boldsymbol{\psi}$)). The Taylor expansion of the latter two terms can be written as follows:

$$\boldsymbol{I}_2 = \sum_{\boldsymbol{n}=0}^{\infty} \boldsymbol{p}_{\boldsymbol{n}}\boldsymbol{cos}\left(\boldsymbol{n} \times 2\boldsymbol{\pi ft} + \boldsymbol{\psi}'_{\boldsymbol{n}}\right) \tag{6}$$

$$\boldsymbol{I}_3 = \boldsymbol{A} \times \left\{\boldsymbol{\phi}\left(\overline{\boldsymbol{\nu}}(\boldsymbol{t})\right) + \sum_{\boldsymbol{h}=1}^{\infty} \frac{\boldsymbol{a}(\boldsymbol{t})^{\boldsymbol{h}}}{2^{\boldsymbol{h}}\boldsymbol{h}!} \frac{\boldsymbol{d}^{\boldsymbol{h}}\boldsymbol{\phi}}{\boldsymbol{d}\boldsymbol{\nu}^{\boldsymbol{h}}}\bigg|_{\boldsymbol{\nu}=\overline{\boldsymbol{\nu}}} \sum_{\boldsymbol{g}=0}^{\boldsymbol{h}} \boldsymbol{C}_{\boldsymbol{h}}^{\boldsymbol{g}}\boldsymbol{cos}[(\boldsymbol{h} - 2\boldsymbol{g})(\boldsymbol{\theta} + \boldsymbol{\psi})]\right\} \tag{7}$$

where $\boldsymbol{p}_{\boldsymbol{n}}$ and $\boldsymbol{\psi}'_{\boldsymbol{n}}$ are functions of $\boldsymbol{i}_{\boldsymbol{m}}(\boldsymbol{t})$ and $\boldsymbol{\psi}_{\boldsymbol{m}}$, and contain information about the IM characteristics, although their specific values are not important here. $\frac{\boldsymbol{d}^{\boldsymbol{h}}\boldsymbol{\phi}}{\boldsymbol{d}\boldsymbol{\nu}^{\boldsymbol{h}}}$ is the h-th derivative of the line shape function, and g is the reduced power expansion coefficient of the cosine formula $\boldsymbol{\theta} = 2\boldsymbol{\pi ft}$.

During data processing, $\boldsymbol{ln}(\boldsymbol{I}_{\boldsymbol{t}}(\boldsymbol{t}))$ is passed through the lock-in amplifier to extract the harmonic signal. Let $h - 2\ g = k$, where k is the order of the harmonic signal. The X component ($\boldsymbol{ln}(\boldsymbol{I}_{\boldsymbol{t}}(\boldsymbol{t})) \times \boldsymbol{cos}(\boldsymbol{k} \times 2\boldsymbol{\pi ft})$) and the Y component ($\boldsymbol{ln}(\boldsymbol{I}_{\boldsymbol{t}}(\boldsymbol{t})) \times \boldsymbol{sin}(\boldsymbol{k} \times 2\boldsymbol{\pi ft})$) of the k-th harmonic signal can be written as:

$$\begin{cases} \boldsymbol{X}_{\boldsymbol{k}} = \frac{1}{2}\boldsymbol{p}_{\boldsymbol{k}}\boldsymbol{cos}(\boldsymbol{\psi}'_{\boldsymbol{k}}) - \frac{1}{2}\boldsymbol{A} \times \sum_{\boldsymbol{g}=0}^{\infty} \left(\frac{(\boldsymbol{a}(\boldsymbol{t})/2)^{\boldsymbol{k}+2\boldsymbol{g}}}{\boldsymbol{g}!(\boldsymbol{k}+\boldsymbol{g})!} \frac{\boldsymbol{d}^{\boldsymbol{k}+2\boldsymbol{g}}\boldsymbol{\phi}}{\boldsymbol{d}\boldsymbol{\nu}^{\boldsymbol{k}+2\boldsymbol{g}}}\Big|_{\boldsymbol{\nu}=\overline{\boldsymbol{\nu}}}\right)\boldsymbol{cos}(\boldsymbol{k\psi}) \\ \boldsymbol{Y}_{\boldsymbol{k}} = -\frac{1}{2}\boldsymbol{p}_{\boldsymbol{k}}\boldsymbol{sin}(\boldsymbol{\psi}'_{\boldsymbol{k}}) + \frac{1}{2}\boldsymbol{A} \times \sum_{\boldsymbol{g}=0}^{\infty} \left(\frac{(\boldsymbol{a}(\boldsymbol{t})/2)^{\boldsymbol{k}+2\boldsymbol{g}}}{\boldsymbol{g}!(\boldsymbol{k}+\boldsymbol{g})!} \frac{\boldsymbol{d}^{\boldsymbol{k}+2\boldsymbol{g}}\boldsymbol{\phi}}{\boldsymbol{d}\boldsymbol{\nu}^{\boldsymbol{k}+2\boldsymbol{g}}}\Big|_{\boldsymbol{\nu}=\overline{\boldsymbol{\nu}}}\right)\boldsymbol{sin}(\boldsymbol{k\psi}) \end{cases} \tag{8}$$

The lock-in amplifier eliminates the effects of $\overline{\boldsymbol{I}}_0$ and G, which means that $\boldsymbol{I}_1$ in Equation (5) becomes zero in the harmonic signal. The two components of any order of harmonic signal are only related to the laser characteristics ($\boldsymbol{i}_{\boldsymbol{m}}(\boldsymbol{t})$ or $\boldsymbol{p}_{\boldsymbol{n}}$, $\boldsymbol{\psi}_{\boldsymbol{m}}$ or $\boldsymbol{\psi}'_{\boldsymbol{n}}$, $\overline{\boldsymbol{\nu}}(\boldsymbol{t})$, $\boldsymbol{a}(\boldsymbol{t})$, and $\boldsymbol{\psi}$) and the absorption signal (detection target). When there is no absorption, that is, when $A = 0$, the transmitted light intensity is the background signal (which is easy to obtain in preparation for testing[10,12,13,16]), and its k-th harmonic signal (which is called the background harmonic signal) component can be written as:

$$\begin{cases} X_k^0 = \frac{1}{2} p_k cos\left(\psi_k'\right) \\ Y_k^0 = -\frac{1}{2} p_k sin\left(\psi_k'\right) \end{cases} \tag{9}$$

Equation (9) shows that the background harmonic signal is related to the IM characteristics ($i_m(t)$/ p_n and ψ_m/ ψ_n') only. After the background harmonic signal is deducted, the k-th harmonic signal (called the absorption harmonic signal) can be written as:

$$\begin{aligned} S_k^a &= \sqrt{\left(X_k - X_k^0\right)^2 + \left(Y_k - Y_k^0\right)^2} \\ &= \frac{1}{2} A \times \left| \sum_{g=0}^{\infty} \left(\frac{(a(t)/2)^{k+2g}}{g!(k+g)!} \frac{d^{k+2g}\phi}{d\nu^{k+2g}} \bigg|_{\nu=\bar{\nu}} \right) \right| \end{aligned} \tag{10}$$

Subtraction of the background harmonic signal eliminates the effects of the IM amplitude ($i_m(t)$ or p_n) and the IM phase (ψ_m or ψ'), and thus I_2 in Equation (5) also becomes zero in the absorption harmonic signal. Because the subtraction and lock-in amplification operation can be interchanged, the background signal ($ln(I_0(t))$) can be subtracted from the natural logarithmic transmitted light intensity ($ln(I_t(t))$) first, and then the harmonic signal is extracted. Finally, the sum of the squares of the two harmonic components eliminates the influence of the FM phase (ψ). Therefore, any order of absorption harmonic signal is solely related to the time-frequency response relationship ($\bar{\nu}$, a) and the absorption signal (detection target).

The time-frequency response relationship ($\bar{\nu}(t)$, $a(t)$) can be obtained using Fabry–Perot (F–P) interferometer monitoring during the experiments; this is common practice in the TDLAS technique.[10–16,23,25] The absorption harmonic signals can then be simulated accurately. The absorption signal includes the integrated absorbance (A) and the line shape derivative ($\frac{d^{k+2g}\phi}{d\nu^{k+2g}}$). Equations (3) and (4) show that the absorption optical path is related linearly to the integrated absorbance only. Therefore, in a uniform flow field, the absorption harmonic signal is related linearly to the optical path. In a non-uniform flow field, the absorption harmonic signal is the absolute value of the integral along the LOS and Equation (10) can then be written as:

$$\begin{aligned} S_k^a = \frac{1}{2} \Bigg| & \int_0^L P(l) X(l) S[T(l)] \\ & \times \sum_{g=0}^{\infty} \left(\frac{(a(t)/2)^{k+2g}}{g!(k+g)!} \frac{d^{k+2g}\phi[P(l), X(l), T(l)]}{d\nu^{k+2g}} \bigg|_{\nu=\bar{\nu}} \right) dl \Bigg| \end{aligned} \tag{11}$$

The LCF-WMS measurement process is illustrated in Figure 1, and includes the following five specific steps:

1. Acquire the background signal in advance during the preparation for the test, and take the natural logarithm of this signal to obtain $ln(I_0(t))$;
2. Take the logarithm of the transmitted light intensity obtained in the experiment (denoted by $ln(I_t(t))$), subtract the $ln(I_0(t))$ term obtained in step 1) from this logarithm, and obtain the measured k-th absorption harmonic signal using a digital lock-in amplifier (LCF − WMS − kf_m);
3. Measure $\bar{\nu}(t)$ and $a(t)$ using an F-P interferometer, and simulate the time-frequency response $\nu(t) = \bar{\nu}(t) + a(t)cos(2\pi ft + \psi)$ (where ψ can have any value);
4. Estimate the initial values of the gas properties, and then calculate the absorption rate modulation signal from the time-frequency response relationship using the Beer–Lambert law. Then, acquire the simulated k-th absorption harmonic signal using the same digital lock-in amplifier that was used in step 2) (LCF − WMS − kf_s);
5. Calculate sum-of-squares error between the simulated and measured values of LCF − WMS − kf. The Levenberg–Marquardt (L–M) algorithm is used to perform the nonlinear fitting iterations and the measured gas properties are obtained after the iteration conditions are met.

3 | EXPERIMENT AND RESULTS

To confirm the viability of the LCF-WMS technique, a demonstration test was performed to measure the water vapor concentration in air at ambient temperature. A schematic of the experimental setup is shown in Figure 2. A distributed feedback (DFB) laser (NLK1E5EAAA, NTT) was used to probe the H_2O transition near 7181 cm^{-1}. A modulation signal composed of a 20 Hz sawtooth wave and a 10 kHz sine wave was generated by a multiple function data acquisition system (DAQ; PCIe-6361, NI). The light that exited the fiber was collimated into a beam via a collimating lens. The transmitted light was then received by a photodiode detector (PDA20CS2, Thorlabs) and the intensity signal was recorded using the same DAQ at a sampling rate of 2 MHz. During the measurement process, the laser time-frequency response is monitored using an F-P interferometer. By moving the detector position along the track, we varied the optical path (the distance from the detector to the collimating lens) from 10 to 40 cm at 10 cm intervals. A temperature and humidity meter (HTC-1) was placed nearby to measure both the temperature and the humidity. An example of measurement data acquired from the 40 cm optical path is shown in Figure 2(B). Figure 2(C) shows the results obtained after taking the natural logarithm of the measurement data. Figure 2(D) shows the simulated absorbance curve near 7181 cm^{-1} with the path length of 40 cm. The peak absorption rate is shown to be approximately 0.65, which is much higher than the traditional weak absorption assumption (<0.05).

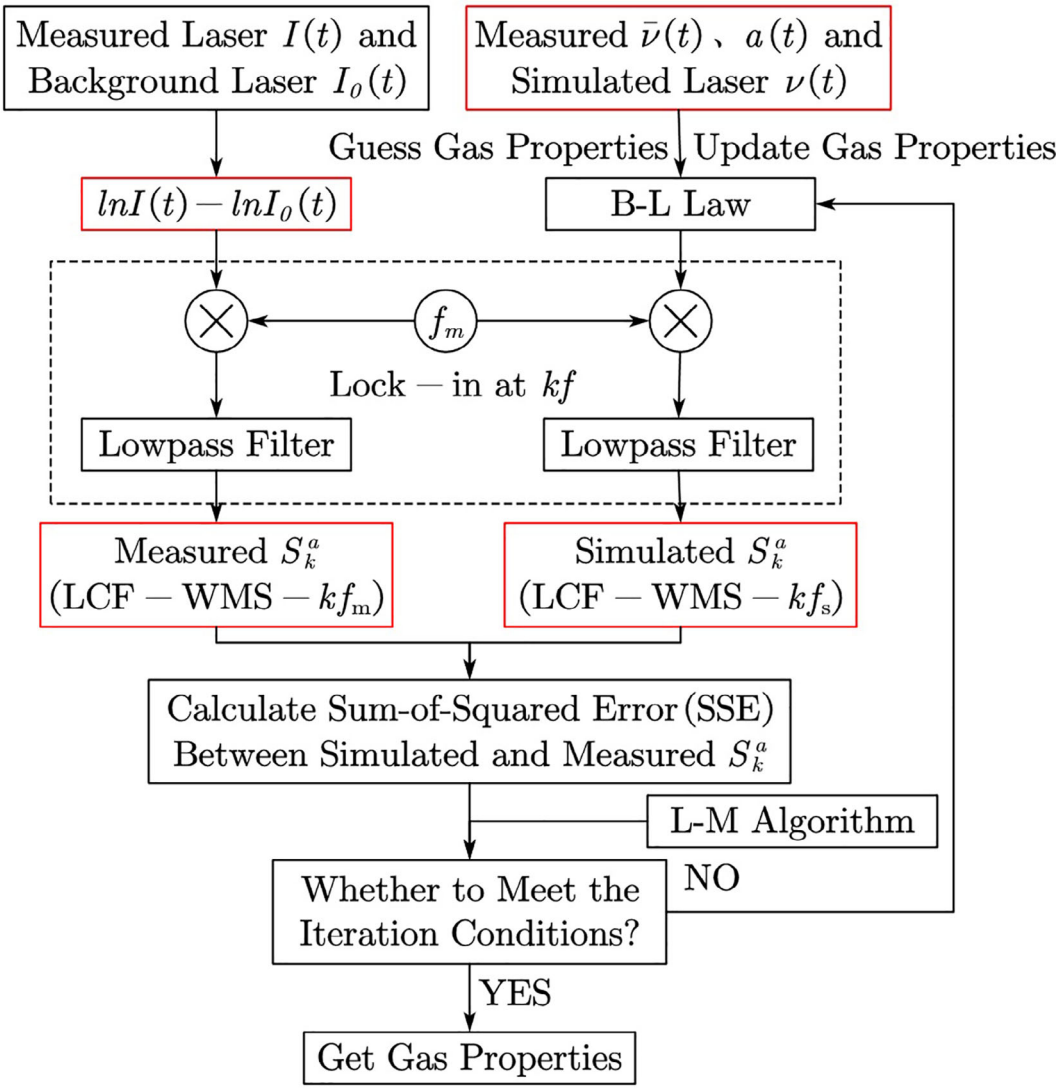

FIGURE 1 Flow chart illustrating the LCF-WMS measurement process [Color figure can be viewed at wileyonlinelibrary.com]

Based on these measurement data, Figure 3(A) shows the first to third harmonic line shapes for the four optical paths obtained using the LCF-WMS method. At each harmonic, the optical path-normalized absorption harmonic signals overlap with each other. These results prove that the entire absorption harmonic signal obtained via the LCF-WMS method is linear with respect to the optical path, that is, LCF-WMS is integrable along the LOS. The slight differences between the first harmonic absorption signals for the different optical paths may be caused by either optical path errors or background harmonic errors. For comparison, Figure 3(B) shows the 2–4*f*/1*f* harmonic line shapes acquired for each optical path using the WMS-*kf*/1*f* method, which is also normalized with respect to the optical path length. The results clearly show that there are significant differences between the 2–4*f*/1*f* harmonic signals in each optical path. Therefore, the harmonic signal obtained by the WMS-*kf*/1*f* method is nonlinear with respect to the optical path, and does not have the property of integrability along the LOS.

Next, for the measurement data obtained from the 40 cm optical path, the LCF-WMS method is used to fit the first to fifth harmonics. The spectrum parameters used are taken from HITRAN2016 database.[26] The fitting results are shown in Figure 4, and the concentration measurement results and the fitting deviation (which is defined as the root mean square ratio of the fitting residual to the peak LCF-WMS-*kf* signal) are given in Table 1. The multiplicative inverse of the fitting deviation is used to characterize the harmonic SNR. The LCF-WMS method's contrast hygrometer concentration measurement deviation does not exceed 5% over the first to fifth harmonics. The measurement deviation is affected by the accuracy of the temperature and humidity meter, the accuracy of the optical path measurement, and the accuracy of the time-frequency response relationship. The fitting deviation does not exceed 0.02 for the first to fifth harmonics, which is mainly because of the very small wavelength scale difference between the simulations and measurements. The fitting residual error is found to increase at

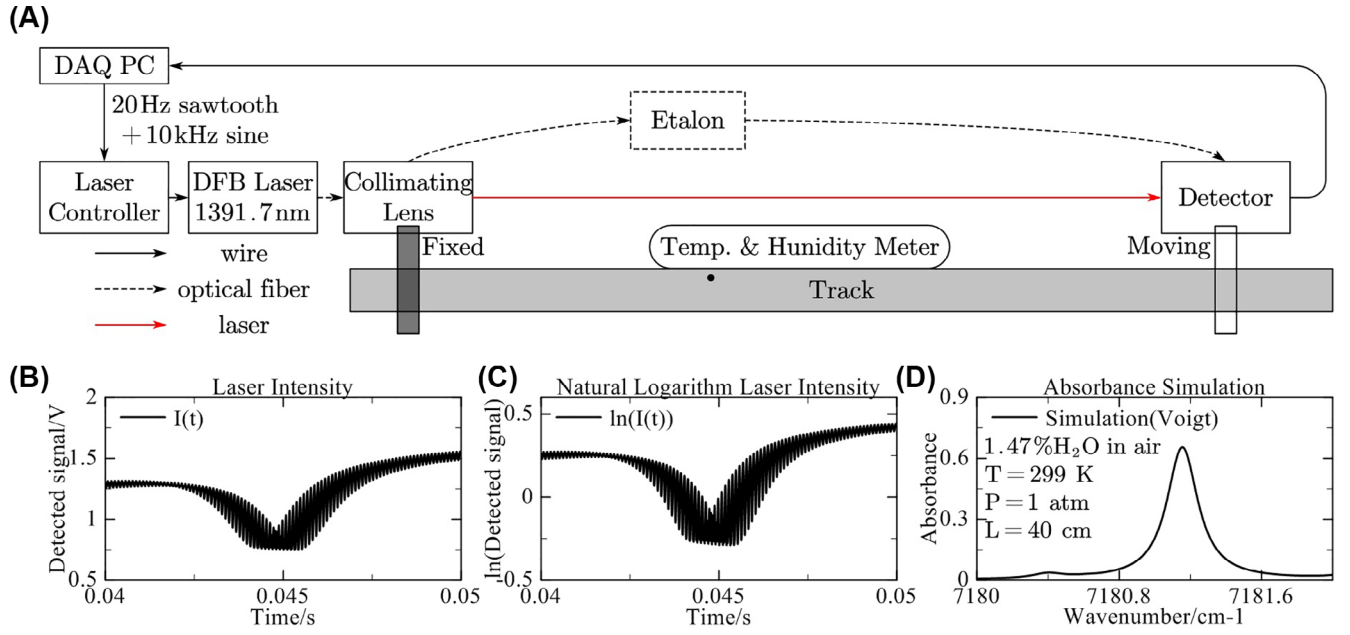

FIGURE 2 (A) Schematic of the experimental setup. (B) Measurement data from the 40 cm optical path. (C) Natural logarithm of the measurement data from the 40 cm optical path. (D) Simulation of the water absorption spectrum near 7181 cm^{-1} under the experimental conditions [Color figure can be viewed at wileyonlinelibrary.com]

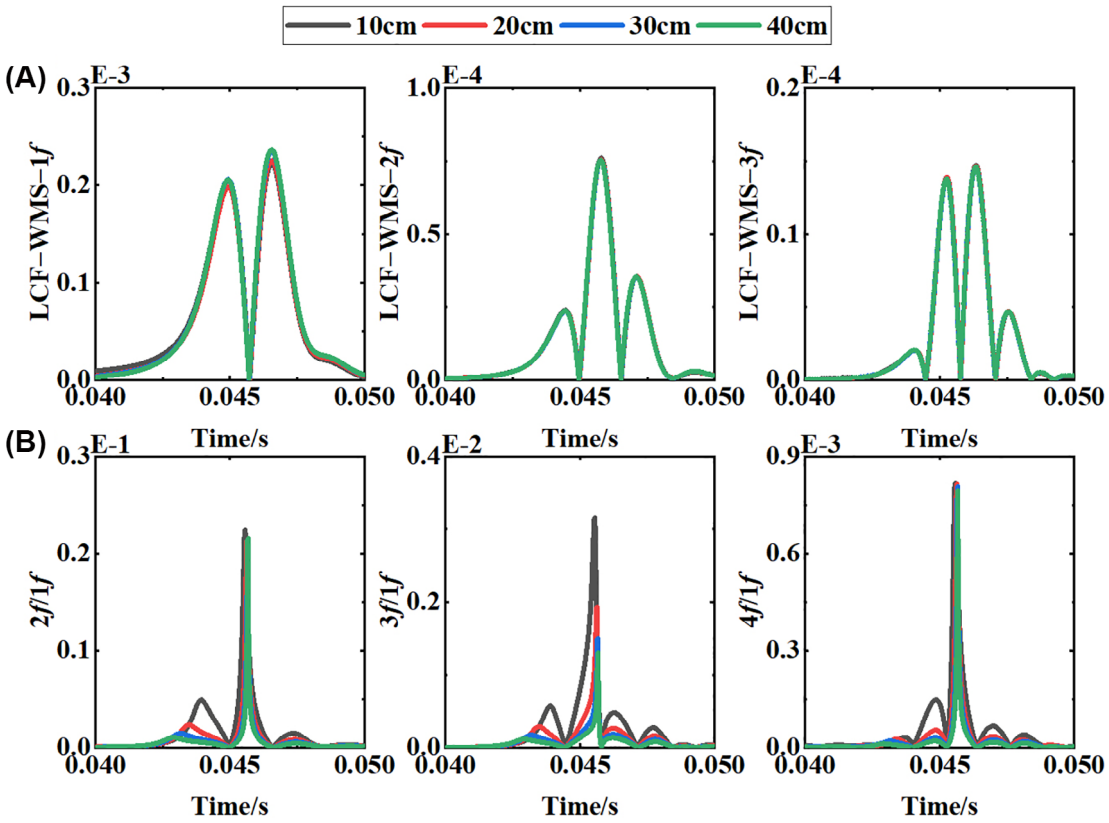

FIGURE 3 (A) First–third harmonic signals for different optical path lengths obtained using the LCF-WMS method (normalized with respect to the optical path length). (B) 2–4*f*/1*f* harmonic signals for different optical path lengths obtained using the *kf*/1*f*-WMS method (normalized with respect to the optical path length) [Color figure can be viewed at wileyonlinelibrary.com]

the harmonic trough. In order to eliminate the influence of IM and achieve the maximum SNR, the second harmonic peak is often used in the traditional WMS for measurement. By contrast, LCF-WMS can use all the signals on the line, not limited to the center wavelength. Certainly, the first harmonic has the largest signal amplitude for measurement.

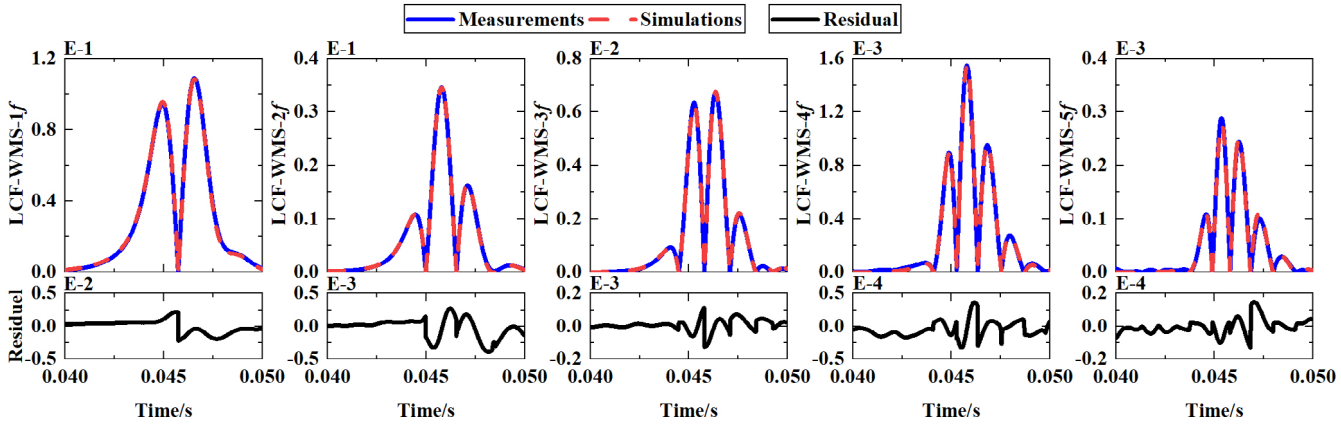

FIGURE 4 LCF-WMS-(1–5)*f* fittings of the measured signal for the 40 cm optical path length [Color figure can be viewed at wileyonlinelibrary.com]

TABLE 1 LCF-WMS-(1-5)*f* concentration measurement results and fitting deviations

	Concentration			
Harmonic order	LCF-WMS	Temperature and humidity meter	Measurement deviation	Fitting deviation
1f	0.01440	0.01472	−2.17%	0.0089
2f	0.01447	0.01472	−1.70%	0.0043
3f	0.01456	0.01472	−1.09%	0.0053
4f	0.01478	0.01472	0.41%	0.0083
5f	0.01539	0.01472	4.55%	0.0158

Nevertheless, the second harmonic still appears to be the best fit among the first to fifth harmonics due to the smallest fitting deviation, which may be attributed to the background harmonic error at the first harmonic. At higher harmonic orders, the fitting deviation becomes larger, which means that the harmonic SNR is reduced. The results show that when the harmonic order is greater than four, the fitting deviation is obvious larger. Therefore, the best SNR may be obtained by using the second or third harmonics in the experiments.

4 | CONCLUSIONS AND OUTLOOK

The LCF-WMS technique has been proposed in this article. By extending the ln-WMS technique and separating the laser intensity characteristics, this method has realized LOS integrability of the harmonic signals for the first time and eliminated the effects of IM and the MP, thus enabling calibration-free measurement. It permits uncertainty quantification by decoupling laser characteristics and absorbing harmonic signals. The results of a water vapor concentration measurement experiment verify that the method is also effective under strong absorption conditions. After comprehensive analysis of the signal amplitude and the fitting deviation, it is recommended that the second or third harmonics are used for fitting, and the relative measurement error does not exceed 2%. The IM separation eliminates the residual modulation amplitude (RMA), so this method may also have a beneficial effect on other modulation absorption spectroscopy technologies[27–31] (such as quartz-enhanced photoacoustic spectroscopy and quartz-enhanced photothermal spectroscopy). And, the combination with the quartz tuning fork detector also may bring a larger range of transition options and a compact measurement system. Because of the integrability of the harmonic signals along the LOS and its baseline-independent data processing capability, this method should offer great advantages for use in absorption tomography and high-pressure environments.

ACKNOWLEDGMENTS

We thank David MacDonald, MSc, from Liwen Bianji (Edanz) (www.liwenbianji.cn/) for editing the English text of a draft of this manuscript.

CONFLICT OF INTEREST

The authors declare no conflicts of interest.

DATA AVAILABILITY STATEMENT

The data that support the findings of this study are available on request from the corresponding author. The data are not publicly available due to privacy or ethical restrictions.

ORCID

Renjie Li https://orcid.org/0000-0002-0860-4760

REFERENCES

[1] Goldenstein CS, Spearrin RM, Jeffries JB, Hanson RK. Infrared laser-absorption sensing for combustion gases. *Prog Energy Combust Sci*. 2017;60:132-176.

[2] Liu C, Xu L. Laser absorption spectroscopy for combustion diagnosis in reactive flows: a review. *Appl Spectrosc Rev*. 2019;54:1-44.

[3] Hanson RK. Applications of quantitative laser sensors to kinetics, propulsion and practical energy systems. *Proc Combust Inst*. 2011;33:1-40.

[4] Li G, Ma K, Jiao Y, et al. Performance enhancement of DFBL based near-infrared CH_4 telemetry system using a focus tunable lens. *Microw Opt Technol Lett*. 2021;63:1147-1151.

[5] Ma L, Li X, Sanders ST, et al. 50-kHz-rate 2D imaging of temperature and H_2O concentration at the exhaust plane of a J85 engine using hyperspectral tomography. *Opt Express*. 2013;21:1152-1162.

[6] Yu X, Yang C-b, Peng J-b, Ma Y-f, Li X-h, Zhang Y-l. Temperature measurement of CH_4/air premix flat flame based on the absorption spectroscopy technology of UV tunable laser. *Spectrosc Spec Anal*. 2016;36:1027-1032.

[7] Goldenstein CS, Jeffries JB, Hanson RK. Diode laser measurements of linestrength and temperature-dependent lineshape parameters of H2O-, CO2-, and N-2-perturbed H2O transitions near 2474 and 2482 nm. *J Quant Spectrosc Radiat Transf*. 2013;130:100-111.

[8] Reid J, Labrie D. 2nd-harmonic detection with tunable diode-lasers-comparison PF experiment and theory. *Appl Phys B: Photophys Laser Chem*. 1981;26:203-210.

[9] Cassidy DT, Reid J. Atmospheric-pressure monitoring of trace gases using tunable diode-lasers. *Appl Optics*. 1982;21:1185-1190.

[10] Rieker GB, Jeffries JB, Hanson RK. Calibration-free wavelength-modulation spectroscopy for measurements of gas temperature and concentration in harsh environments. *Appl Optics*. 2009;48:5546-5560.

[11] Peng Z, Ding Y, Che L, Li X, Zheng K. Calibration-free wavelength modulated TDLAS under high absorbance conditions. *Opt Express*. 2011;19:104-110.

[12] Sun K, Chao X, Sur R, Goldenstein CS, Jeffries JB, Hanson RK. Analysis of calibration-free wavelength-scanned wavelength modulation spectroscopy for practical gas sensing using tunable diode lasers. *Meas Sci Technol*. 2013;24:125203.

[13] Goldenstein CS, Strand CL, Schultz IA, Sun K, Jeffries JB, Hanson RK. Fitting of calibration-free scanned-wavelength-modulation spectroscopy spectra for determination of gas properties and absorption lineshapes. *Appl Optics*. 2014;53:356-367.

[14] Upadhyay A, Chakraborty AL. Calibration-free 2f WMS with in situ real-time laser characterization and 2f RAM nulling. *Opt Lett*. 2015;40:4086-4089.

[15] Du Y, Peng Z, Ding Y. Wavelength modulation spectroscopy for recovering absolute absorbance. *Opt Express*. 2018;26:9263-9272.

[16] Qu ZC, Ghorbani R, Valiev D, Schmidt FM. Calibration-free scanned wavelength modulation spectroscopy-application to H_2O and temperature sensing in flames. *Opt Express*. 2015;23:492-499.

[17] Yang C, Mei L, Wang X, et al. Simultaneous measurement of gas absorption and path length by employing the first harmonic phase angle method in wavelength modulation spectroscopy. *Opt Express*. 2020;28:3289-3297.

[18] Sun K, Chao X, Sur R, Jeffries JB, Hanson RK. Wavelength modulation diode laser absorption spectroscopy for high-pressure gas sensing. *Appl Phys B Lasers Opt*. 2013;110:497-508.

[19] Cai W, Kaminski CF. Multiplexed absorption tomography with calibration-free wavelength modulation spectroscopy. *Appl Phys Lett*. 2014;104:154106.

[20] Guha A, Schoegl IM. Tomographic imaging of flames: assessment of reconstruction error based on simulated results. *J Propul Power*. 2014;30:350-359.

[21] Cai W, Kaminski CF. Tomographic absorption spectroscopy for the study of gas dynamics and reactive flows. *Prog Energy Combust Sci*. 2017;59:1-31.

[22] Li S, Sun L. Natural logarithm wavelength modulation spectroscopy. *Chin Opt Lett*. 2021;19:031201.

[23] Li S, Sun L. Natural logarithm wavelength modulation spectroscopy: a linear method for any large absorbance. *Spectrochim Acta Part A*. 2021;254:119601.

[24] Nie W, Xu Z, Rao G, et al. Methods of tunable diode laser absorption saturation spectroscopy to gas sensing under optically thick conditions. *Microw Opt Technol Lett*. 2021;63:2063-2067.

[25] Liu JX, Zhou YT, Guo SJ, et al. A novel methodology to directly pre-determine the relative wavelength response of DFB laser in wavelength modulation spectroscopy. *Opt Express*. 2019;27:1249-1261.

[26] Gordon IE, Rothman LS, Hill C, et al. The HITRAN2016 molecular spectroscopic database. *J Quant Spectrosc*. 2017;203:3-69.

[27] Ma Y, Lewicki R, Razeghi M, Tittel FK. QEPAS based ppb-level detection of CO and N2O using a high power CW DFB-QCL. *Opt Express*. 2013;21:1008-1019.

[28] Ma Y, He Y, Tong Y, Yu X, Tittel FK. Quartz-tuning-fork enhanced photothermal spectroscopy for ultra-high sensitive trace gas detection. *Opt Express*. 2018;26:103-110.

[29] Ma Y, Hu Y, Qiao S, He Y, Tittel FK. Trace gas sensing based on multi-quartz-enhanced photothermal spectroscopy. *Photoacoustics*. 2020;20:206.

[30] Lang Z, Qiao S, He Y, Ma Y. Quartz tuning fork-based demodulation of an acoustic signal induced by photo-thermo-elastic energy conversion. *Photoacoustics*. 2021;22:100272.

[31] Qiao S, He Y, Ma Y. Trace gas sensing based on single-quartz-enhanced photoacoustic-photothermal dual spectroscopy. *Opt Lett*. 2021;46:2449-2452.

How to cite this article: Li R, Li F, Lin X, Yu X. Linear calibration-free wavelength modulation spectroscopy. *Microw Opt Technol Lett*. 2021;1–7. https://doi.org/10.1002/mop.33063